Electronic supplementary information

Bimetallic Ru(II) and Os(II) complexes based on pyrene-bisimidazole spacer: synthesis, photophysics, electrochemistry and multisignalling DNA binding studies in the near infrared region

Sourav Mardanya, Debiprasad Mondal, and Sujoy Baitalik*

Department of Chemistry, Inorganic Chemistry Section, Jadavpur University, Kolkata – 700032, India

Physical measurements

Elemental analyses of the compounds were performed with a Vario-Micro V2.0.11 elemental (CHNSO) analyzer. NMR spectra were collected on Bruker 500 spectrometer in DMSO-d_6, and high resolution mass spectroscopy was performed on a Waters Xevo G2 QTOf mass spectrometer. The UV/vis absorption spectra were recorded with a Shimadzu UV 1800 spectrometer. A matched pair of quartz cuvettes (path length 1 cm) was employed. Steady state luminescence spectra were obtained either by a Perkin–Elmer LS55 or Spex fluorolog-2 spectrofluorometer equipped with DM3000F software. Luminescence quantum yields were determined by using literature method taking $[Ru(bpy)_3]^{2+}$ as the standard. Luminescence lifetime measurements were carried out by using time–correlated single photon counting set up from Horiba Jobin-Yvon. The luminescence decay data were collected on a Hamamatsu MCP photomultiplier (R3809) and were analyzed by using IBH DAS6 software. Cyclic and square-wave voltammetric experiments were performed in deaerated acetonitrile with a BAS epsilon electrochemistry system and a three-electrode set up consisting of a platinum or glassy carbon working electrode, a platinum counter electrode, and Ag/AgCl reference electrode. Tetraethylammonium perchlorate (TEAP) was used as background electrolyte. The potentials reported in this study were referenced against the Ag/AgCl electrode, which under the given experimental conditions gave a value of 0.36 V for the Fc/Fc^+ couple. Spectroelectrochemical measurements were performed with a system consisting of a BAS epsilon potentiostat/galvanostat, a Shimadzu 3600 UV-VIS-NIR spectrophotometer and an optically transparent spectroelectrochemical cell specially designed by BAS.

X-ray crystallographic analyses

The crystallographic data, details of data collection, and refinement parameter for the complex **1** are summarized in Table S1. Single crystal of suitable size was obtained by diffusing toluene to 1:1 acetonitrile-dichloromethane solution of the complex. The crystal was immersed in paratone oil and then mounted on the tip of a glass fibre and cemented using epoxy resin. Intensity data for the crystal was collected using MoKα (λ = 0.7107 Å) radiation on a Bruker SMART APEX II diffractometer equipped with CCD area detector at room temperature. The data integration and reduction were processed with SAINT[S1] software provided with the software package of SMART APEX II. An empirical absorption correction was applied to the collected reflections with SADABS. [S1] The structure was solved by direct methods using SHELXTL[S2] and was refined on F^2 by the full-matrix least-squares technique

using the SHELXL-97 [S3] program package. Graphics was generated using PLATON.[S4] Non-hydrogen atoms were refined anisotropically until the convergence. All the hydrogen atoms were geometrically positioned and treated as riding atoms.

Theoretical computational methods

Quantum chemical calculations were performed with the Gaussian 09 program [S5] employing the DFT method with Becke's three-parameter hybrid functional and Lee-Yang-Parr's gradient corrected correlation functional B3LYP level of theory.[S6,S7] The 6-31G(d) basis set was employed for the C, H and N while SDD basis set was used for Ru and Os atoms.[S8] Geometries were fully optimized using the criteria of the respective programs. Time-dependent DFT (TD-DFT) calculations were performed to assign the experimentally observed bands in the complexes.[S9-S12] The excitation energies, computed within the acetonitrile solvent simulated by the CPCM model, [S13] has been determined by using the so-called nonequilibrium approach, which has been designed for the study of the absorption process.[S14,S15] Only singlet-singlet transitions, that is, the spin-allowed transitions, have been taken into account. UKS calculations were also performed to calculate singlet-triplet energy gap in CH_3CN using the CPCM model. Orbital analysis was completed with Gauss View[S16] and Gauss sum 2.2.[S17]

DNA binding experiments

Absorption and emission spectral experiments

UV-vis absorption and emission titrations were carried out by maintaining a constant metal complex concentration (20 μM) and adding incrementally the CT-DNA solution of appropriate concentration in 5 mM Tris-HCl/NaCl buffer with the ionic strength of 50 .0 × 10^{-3} m (pH 7.30) at room temperature. After each addition of DNA to the solution of the metal complexes, the resulting solution was allowed to equilibrate at 25 °C for 5 min, after which the absorption and emission readings were noted. Proper corrections were made to the absorbance of CT-DNA. The equilibrium binding constant (K_b) and the binding site size (s, per base pair) of the complexes to CT-DNA were calculated by non-linear least square analysis of the isotherm using the expression of Bard and co-workers based on the McGhee-von Hippel (MvH) model.[S18-S19]

$$(\varepsilon_a - \varepsilon_f)/(\varepsilon_b - \varepsilon_f) = (b - (b^2 - 2K_b^2C_t[DNA]/s)^{1/2})/2K_bC_t \quad (S1)$$

$$(I_a - I_f)/(I_b - I_f) = (b - (b^2 - 2K_b^2C_t[DNA]/s)^{1/2})/2K_bC_t \quad (S2)$$

where b = 1 + K_bC_t + K_b[DNA]/2s, ε_a is the extinction coefficient observed for the spectral band at a given DNA concentration, ε_f is the extinction coefficient of the free complex in solution, ε_b is the extinction coefficient of the complex when fully bound to DNA. Similarly I_a, I_f and I_b are the luminescence intensities of the complex at a given DNA concentration, free complex and fully bound to DNA respectively. K_b is the equilibrium binding constant, C_t is the total complex concentration, [DNA] is the DNA concentration in nucleotides and s is the binding site size of the complexes in base pairs. The non-linear least-square fit analysis was done using Origin Lab software. The lifetimes of the complexes were also recorded as a function of CT-DNA in 5 mM Tris-HCl/ NaCl buffer with the ionic strength of 50 .0 × 10^{-3} m (pH 7.30) at room temperature.

Competitive binding fluorescence experiments

The apparent binding constants (K_{app}) of the complexes have been evaluated by using ethidium bromide (EB)-bound CT-DNA solution in 5 mM Tris-HCl/ NaCl buffer with the ionic strength of 50 .0 × 10^{-3} m (pH 7.30) at room temperature. The luminescence intensities at 602 nm (546 nm excitation) of EB-DNA conjugate with increasing concentration of **1** and **2** were recorded. The K_{app} values were calculated by using the equation K_{EB} × [EB] = K_{app} × [complex], where K_{EB} is the binding constant of EB (K_{EB} = 1.25 × 10^6 M^{-1}), [EB] is the concentration of EB (13 μM) and [complex] is the concentration of the complex at 50% reduction of the initial fluorescence emission intensity.[S20]

Circular dichroism experiments

The Circular dichroism (CD) spectroscopy was studied on a JASCO J-815 CD spectropolarimeter between 400 and 200 nm in continuous scanning mode at 25°C. Experiments were performed by adding progressively increasing amounts of complexes to the solutions of CT-DNA [40μM] in 5 mM Tris-HCl/ NaCl buffer with the ionic strength of 50 .0 × 10^{-3} m (pH 7.30).

Thermal denaturation experiments

The effect of temperature on CT-DNA in absence and presence of the complexes were measured from circular dichroism study. The experiments were performed on a JASCO J-815 CD spectropolarimeter equipped with a Peltier temperature-controller (JASCO-PTC-423S/15). CD melting profiles were generated by rising temperature from 40 to 110C with

monitoring the absorbance at 260nm in 5 mM Tris-HCl/ NaCl buffer with the ionic strength of 50 .0 × 10^{-3} m (pH 7.30) medium. The melting temperature *T*m was taken as the midpoint of the melting curve which was obtained from the maximum of the first derivative plot and checked graphically by tangent method. Δ*T*m value was calculated by subtracting *T*m of the free nucleic acid from that of the complex.[S21]

Molecular docking studies

Molecular docking studies were performed using HEX 8.0 software.[S22] To perform such studies, crystal structure of B-DNA (PDB ID: 1BNA) and DFT optimized structures (using Gaussian 09 software) of the complexes were used. The crystal structure of B-DNA was retrieved from the protein data bank (http://www.rcsb.org./pdb). To obtain the molecular docked structures and to elucidate different type of interaction processes between DNA and the receptors Biovia Discovery Studio 2016 software was used.

Viscometric study

The viscosity of sonicated DNA[S23] was measured by a fabricated micro viscometer, maintained at 28 (±0.5) °C in a thermostatic water bath. Then the viscosities of CT-DNA-EB, CT-DNA-Complex **1** and CTDNA-Complex **2** conjugates were measured in the same experimental conditions. Data were presented as $(\eta/\eta_o)^{1/3}$ versus the ratio of the concentration of either EB or complex **1** or **2** to that of the CT DNA, where η_o is the viscosity of CT DNA solution alone and η is the viscosity of CT DNA solution in the presence of either the complexes or EB. Viscosity values were calculated from the observed flow time of CT DNA by the relation $\eta = t - t_0$, where t and t_0 are the values of flow times for the solution and the Tris-NaCl buffer respectively.

Table S1 Crystallographic data for complex **1**

Compound	**1**
Formula	C75 H56 Cl4 N14 O16 Ru2
fw	1753.28
T (K)	293(2)
Cryst. Syst.	Triclinic
Space group	P-1
a (Å)	12.2111(5)
b (Å)	18.6407(6)
c (Å)	18.8598(8)
α (deg)	75.740(3)
β (deg)	77.216(4)
γ (deg)	80.547(3)
V (Å^3)	4030.1(3)
Dc(g cm^{-3})	1.445
Z	2
μ (mm^{-1})	0.580
F(000)	1776.0
θ range (deg)	1.72-25.00
Data/restraints/params	14064/0/1001
GOF on F^2	1.003
R_1 [$I > 2\sigma(I)$][a],	0.0656
wR_2 (all data)[b]	0.1423
$\Delta\rho_{max}/\Delta\rho_{min}$ (e Å)	1.846/ -1.533
[a]R1(F) = [$\sum$ || F_0 | - |F_C || / $\sum$ | F_0], [b]wR2 (F^2) = [$\sum w(F_0^2 - F_C^2)^2 / \sum w(F_0^2)^2$]$^{1/2}$	

Table S2 Selected calculated bond distances (Å) for **1** and **2** in ground and UKS optimized state along with available X-ray crystal data

	Exp **1**	Soln. **1**	UKS **1**		Soln. **2**	UKS **2**
Ru1-N1	2.08(5)	2.11	2.12	Os1-N1	2.11	2.12
Ru1-N2	2.14(4)	2.21	2.21	Os1-N2	2.20	2.20
Ru1-N8	2.04(5)	2.10	2.09	Os1-N8	2.10	2.10
Ru1-N7	2.06(5)	2.10	2.13	Os1-N7	2.10	2.13
Ru1-N9	2.04(5)	2.09	2.06	Os1-N9	2.09	2.08
Ru1-N10	2.04(4)	2.07	2.05	Os1-N10	2.08	2.07
Ru2-N4	2.16(4)	2.21	2.21	Os2-N4	2.20	2.20
Ru2-N6	2.10(4)	2.11	2.11	Os2-N6	2.12	2.12
Ru2-N14	2.07(5)	2.10	2.10	Os2-N14	2.10	2.10
Ru2-N13	2.05(5)	2.10	2.10	Os2-N13	2.10	2.10
Ru2-N12	2.05(5)	2.09	2.09	Os2-N12	2.09	2.09
Ru2-N11	2.04(4)	2.07	2.07	Os2-N11	2.08	2.08

Table S3 Selected calculated bond angles (°) for **1** and **2** in ground and UKS optimized state along with available X-ray crystal data

	1				**2**		
	Exp **1**	Soln. **1**	UKS **1**			Soln. **2**	UKS **2**
N1-Ru1-N2	78.20(17)	77.82	77.60		N1-Os1-N2	77.10	77.11
N1-Ru1-N8	172.33(19)	173.69	173.73		N1- Os1-N8	173.39	173.87
N1-Ru1-N7	93.74(19)	96.33	98.14		N1- Os1-N7	96.69	98.69
N1-Ru1-N9	92.11(18)	88.43	86.36		N1- Os1-N9	88.14	86.36
N1-Ru1-N10	94.88(19)	93.98	93.33		N1- Os1-N10	94.50	93.93
N2-Ru1-N8	100.25(17)	103.81	105.87		N2- Os1-N8	104.56	106.28
N2-Ru1-N7	87.82(17)	86.54	84.46		N2- Os1-N7	85.95	84.34
N2-Ru1-N9	96.79(18)	97.50	98.37		N2- Os1-N9	98.16	98.57
N2-Ru1-N10	172.08(18)	171.01	170.85		N2- Os1-N10	170.85	170.88
N8-Ru1-N7	78.66(19)	77.78	77.20		N8- Os1-N7	77.14	76.78
N8-Ru1-N9	95.54(19)	97.32	98.14		N8- Os1-N9	97.88	98.03
N8-Ru1-N10	87.12(19)	84.72	83.25		N8- Os1-N10	84.19	82.78
N7-Ru1-N9	173.19(19)	174.32	175.11		N7- Os1-N9	174.26	174.63
N7-Ru1-N10	96.54(18)	98.12	98.21		N7- Os1-N10	98.77	98.85
N9-Ru1-N10	79.48(18)	78.41	79.59		N9- Os1-N10	77.70	78.93
N4-Ru2-N12	169.38(18)	170.96	170.86		N4-Os2-N12	170.75	170.77
N4-Ru2-N14	103.08(17)	103.89	104.00		N4- Os2-N14	104.66	104.64
N4-Ru2-N11	94.86(18)	97.46	97.31		N4- Os2-N11	98.08	98.00
N4-Ru2-N13	90.08(18)	86.56	86.64		N4- Os2-N13	86.01	86.04
N6-Ru2-N4	78.44(17)	77.81	77.79		N6- Os2-N4	77.10	77.08
N6-Ru2-N14	176.46(18)	173.70	173.62		N6- Os2-N14	173.41	173.29
N6-Ru2-N13	97.38(18)	96.36	96.30		N6- Os2-N13	96.74	96.62
N6-Ru2-N11	88.25(18)	88.43	88.45		N6- Os2-N11	88.14	88.19
N6-Ru2-N12	92.12(18)	93.94	93.91		N6- Os2-N12	94.42	94.49
N13-Ru2-N11	173.17(19)	174.13	174.37		N13- Os2-N11	174.23	174.31
N13-Ru2-N12	96.01(19)	98.15	98.21		N13- Os2-N12	98.80	98.83
N11-Ru2-N12	79.85(19)	78.41	78.42		N11- Os2-N12	77.70	77.71
N14-Ru2-N13	79.47(18)	77.78	77.78		N14- Os2-N13	77.15	77.14
N14-Ru2-N11	94.78(18)	97.29	97.31		N14- Os2-N11	97.81	97.89
N14-Ru2-N12	86.63(18)	84.69	84.64		N14- Os2-N12	84.16	84.14

Table S4 Selected molecular orbital along with their energies and compositions for **1** and **2** in solution phase

	Energy/ eV	(%) Composition			
		1 (%) Composition			
MO	**1**	Ru^{II}	pyrene imida	pyridine	bpy
LUMO+3	-2.59	5.33	12.02	12.49	70.14
LUMO+2	-2.61	6.27	3.52	1.06	89.13
LUMO+1	-2.65	2.06	9.13	7.10	81.68
LUMO	-2.65	1.81	6.68	5.48	86.02
HOMO	-5.93	23.83	65.59	7.25	3.30
HOMO-1	-6.09	80.08	5.59	3.44	10.87
HOMO-2	-6.18	60.22	26.06	5.06	8.64
HOMO-3	-6.27	73.44	10.11	3.52	12.91
		2 (%) Composition			
MO	**2**	Os^{II}	pyrene imida	pyridine	bpy
LUMO+3	-2.58	8.02	12.25	12.99	66.73
LUMO+2	-2.59	8.42	11.97	6.42	73.17
LUMO+1	-2.71	1.60	13.26	15.97	69.15
LUMO	-2.72	1.63	10.42	12.96	74.96
HOMO	-5.77	65.64	19.23	4.64	10.47
HOMO-1	-5.81	79.23	4.54	3.75	12.46
HOMO-2	-6.04	70.77	8.67	4.58	15.96
HOMO-3	-6.05	67.74	10.08	5.49	16.67

Table S5 Selected molecular orbital along with their energies and compositions for **1** and **2** in UKS optimized state

	Energy/ eV	(%) Composition			
		1 (%) Composition			
MO	**1**	Ru^{II}	pyrene imida	pyridine	bpy
LUMO+3	-2.61	5.94	4.11	4.86	85.07
LUMO+2	-2.66	1.66	6.09	9.03	83.21
LUMO+1	-2.86	2.37	38.44	57.61	1.55
LUMO	-2.95	2.90	0.51	0.15	96.42
HOMO	-3.89	3.81	10.91	0.51	84.75
HOMO-1	-6.02	38.25	49.99	6.45	5.29
HOMO-2	-6.19	44.93	42.48	6.02	6.54
HOMO-3	-6.30	75.12	8.95	2.53	13.39
		2 (%) Composition			
MO	**2**	Os^{II}	pyrene imida	pyridine	bpy
LUMO+3	-2.64	4.31	20.57	26.06	49.03
LUMO+2	-2.89	4.54	31.17	45.31	18.97
LUMO+1	-2.94	5.60	3.85	5.09	85.45
LUMO	-3.15	3.50	7.61	4.67	84.02
HOMO	-3.38	3.80	8.45	4.01	83.71
HOMO-1	-6.00	53.86	30.14	5.43	10.54

HOMO-2	-6.16		67.05	11.44	5.54	15.96
HOMO-3	-6.20		31.92	58.09	4.54	5.42

Table S6 Binding constants of **1** and **2** with DNA in 50mM, 300mM and 1000mM ionic strength tris buffer solution (pH=7.30)

Complex	From Absorption(K_b)	From Emission(K_b)
Strength 50 mM		
1	K_b = (7.23±0.59)×10^6 M^{-1} s = 2.07±0.02	K_b = (7.04±0.65)×10^6 M^{-1} s =1.98±0.02
2	K_b=(7.51±0.65)×10^6 M^{-1} s = 1.96±0.02	K_b=7.74±0.64×10^6 M^{-1} s=1.99 ±0.01
Strength 300 mM		
1	K_b = (7.62±0.17)×10^5 M^{-1} s = 2.04±0.05	K_b = (7.72±0.14)×10^5 M^{-1} s = 1.99±0.02
2	K_b = (8.14±0.14)×10^5 M^{-1} s = 2.06±0.03	K_b = (8.04±0.08)×10^5 M^{-1} s = 1.98±0.05
Strength 1000 mM		
1	K_b = (3.14±0.21)×10^5 M^{-1} s = 1.99±0.08	K_b = (3.32±0.19)×10^5 M^{-1} s = 2.03±0.04
2	K_b = (4.24±0.17)×10^5 M^{-1} s = 2.09±0.02	K_b = (4.76±0.11)×10^5 M^{-1} s = 2.10±0.02

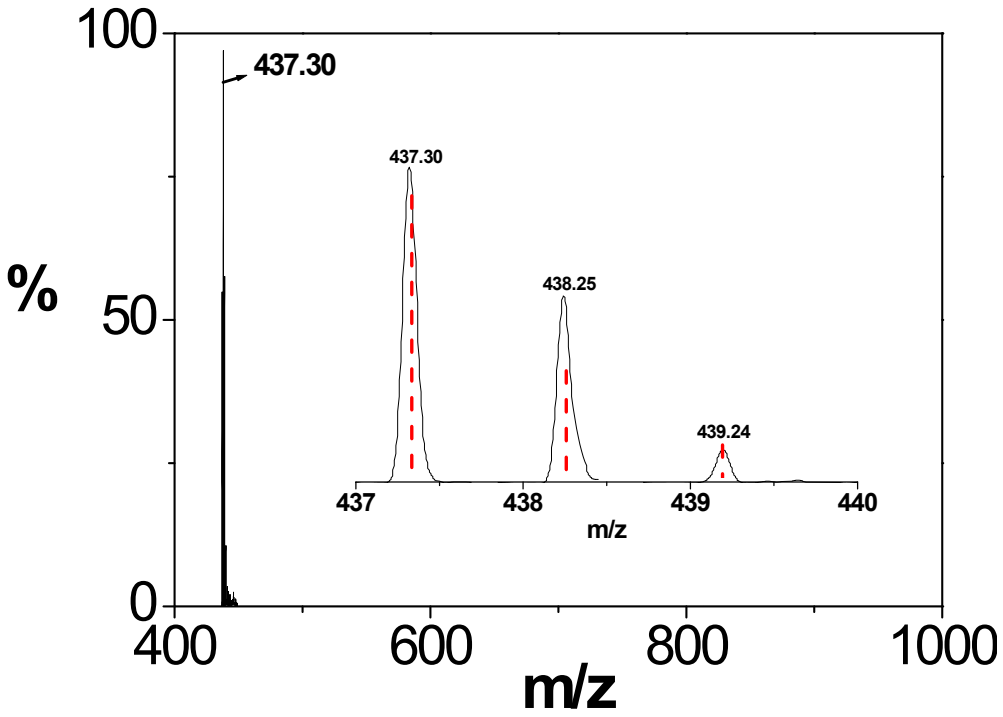

Fig. S1 ESI-MS (positive) for the cation $H_3Imz_2PPy_2^+$ (*m/z* = 437.30) in acetonitrile showing the observed and isotopic distribution patterns.

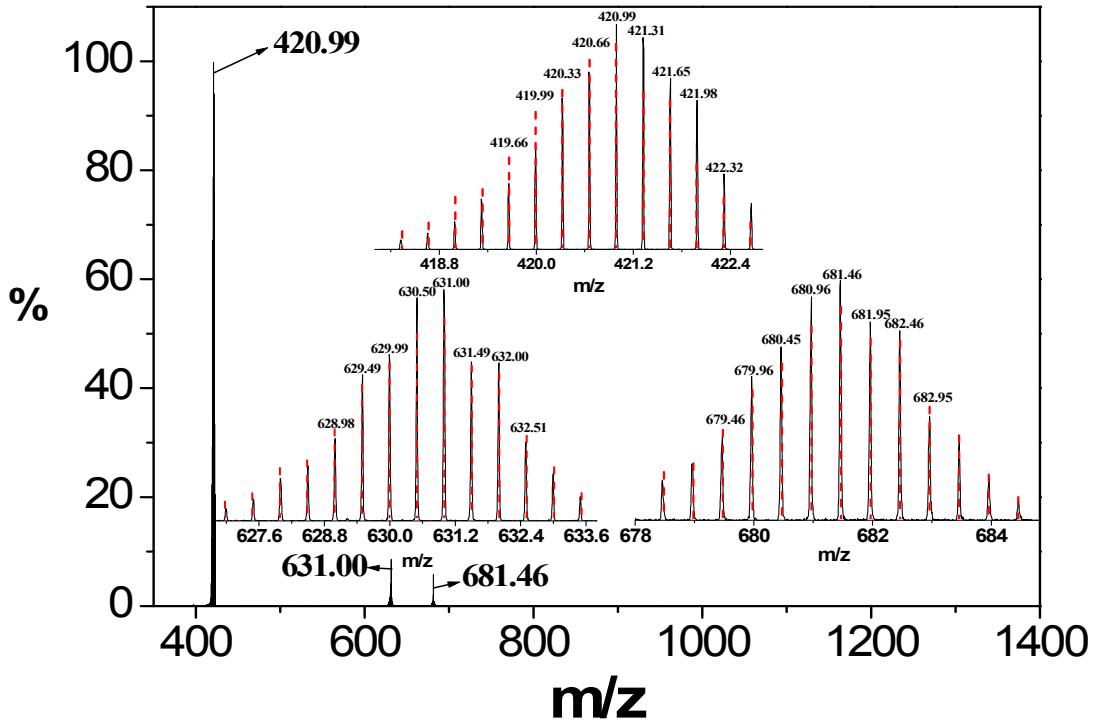

Fig. S2 ESI-MS (positive) for the complex cations of **1**, $[(bpy)_2Ru(HImz_2PPy_2)Ru\ (bpy)_2]^{3+}$ (*m/z* = 420.99), $[(bpy)_2Ru(Imz_2PPy_2)Ru(bpy)_2]^{2+}$ (*m/z* = 631.00) and $[(bpy)_2\ Ru\ (HImz_2PPy_2)\ Ru(bpy)_2(ClO_4)]^{2+}$ (*m/z* = 681.46) in acetonitrile showing both experimental and simulated isotopic distribution patterns.

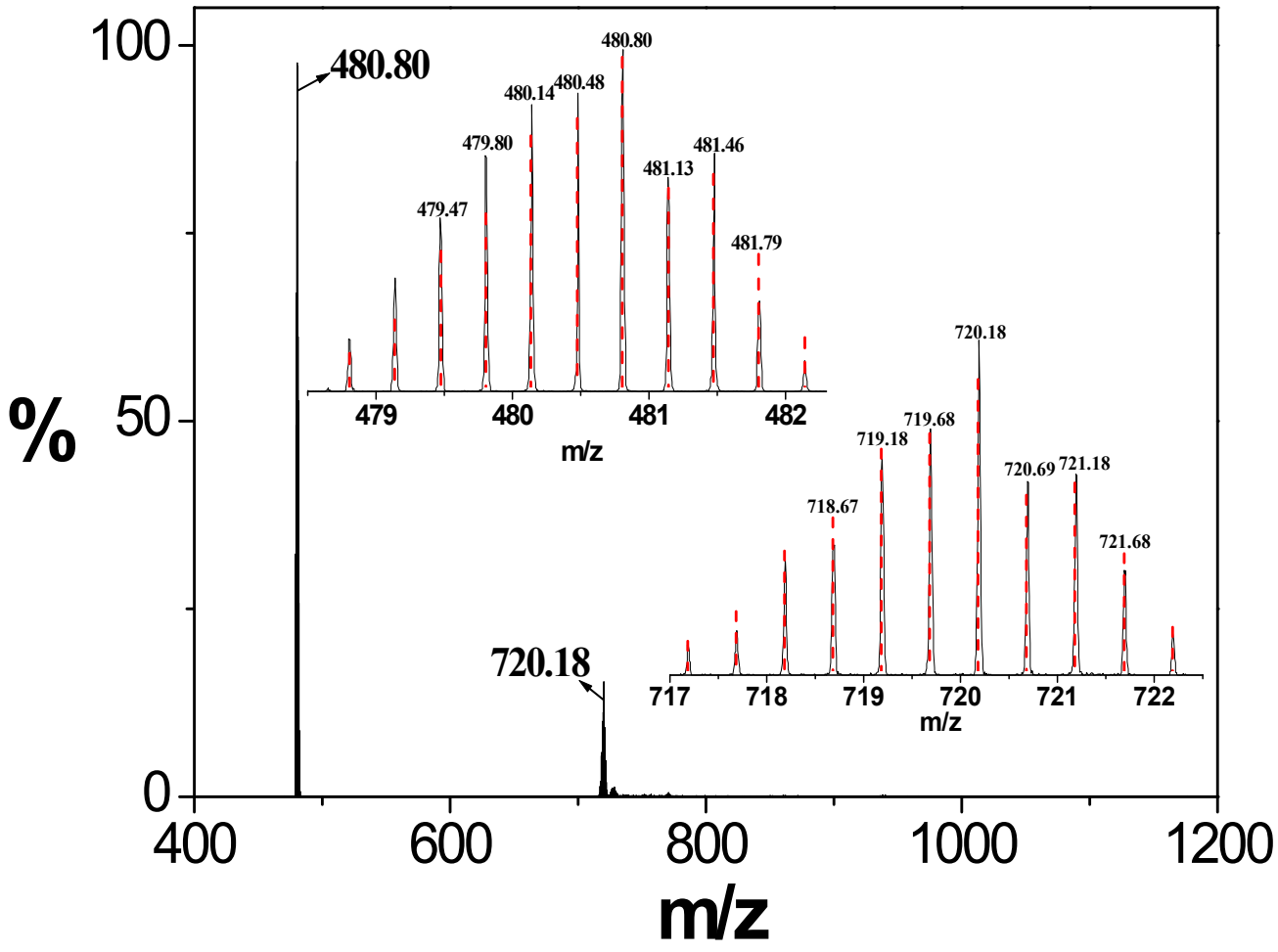

Fig. S3 ESI-MS (positive) for the complex cations of **2,** $[(bpy)_2Os(HImz_2PPy_2)Os(bpy)_2]^{3+}$ (*m/z* = 480.80), $[(bpy)_2Os(Imz_2PPy_2)Os(bpy)_2]^{2+}$ (*m/z* = 720.18) in acetonitrile showing the observed and isotopic distribution patterns.

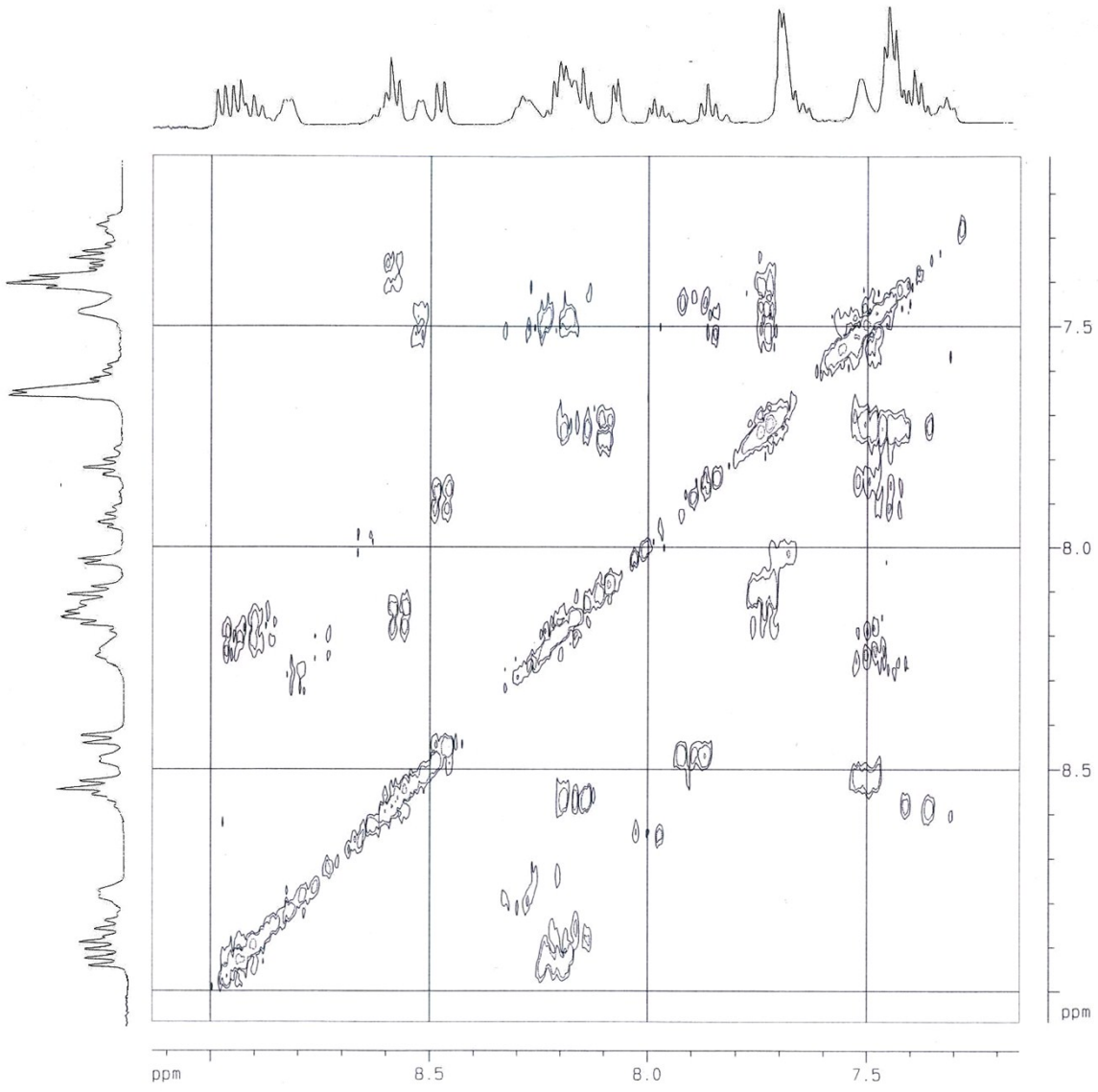

Fig. S4 ^{1}H-^{1}H COSY NMR spectrum of **1** in DMSO-d_6.

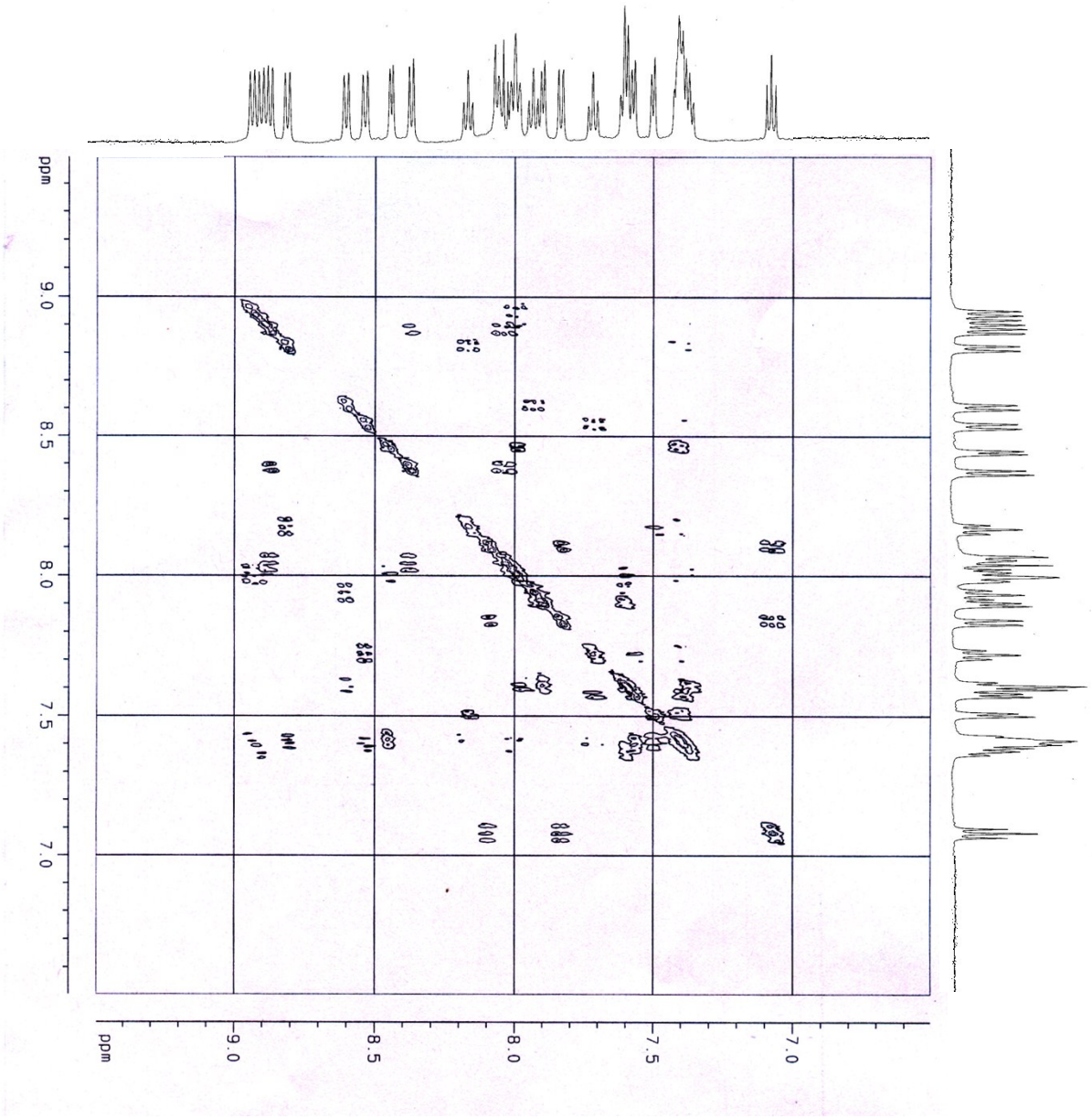

Fig. S5 ^{1}H-^{1}H COSY NMR spectrum of **2** in DMSO-d_6.

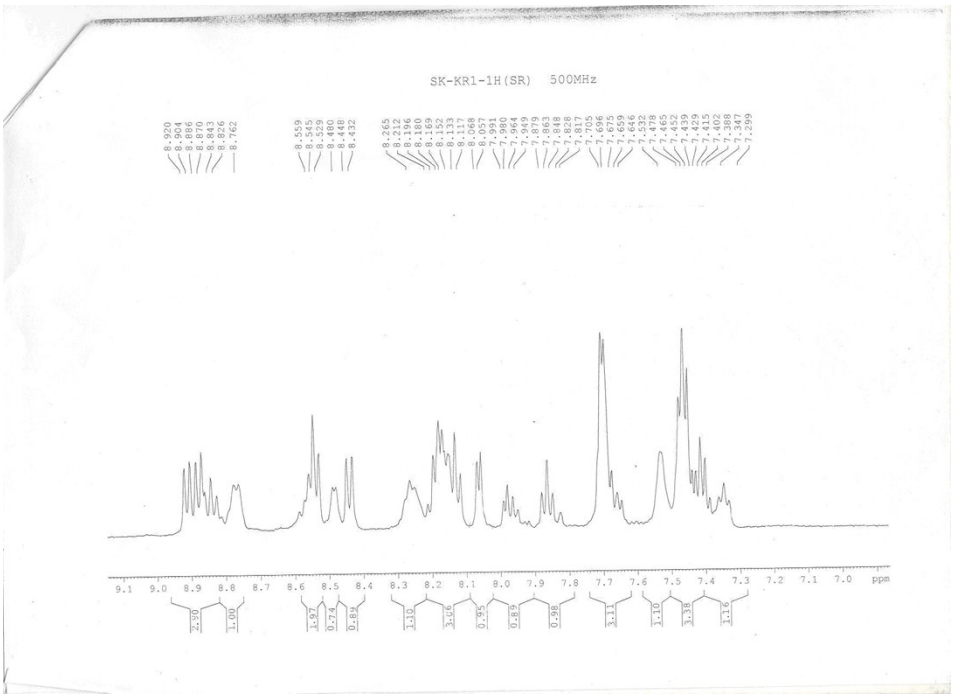

Fig. S6 Scanned ^{1}H NMR spectrum of complex **1** in DMSO-d_6

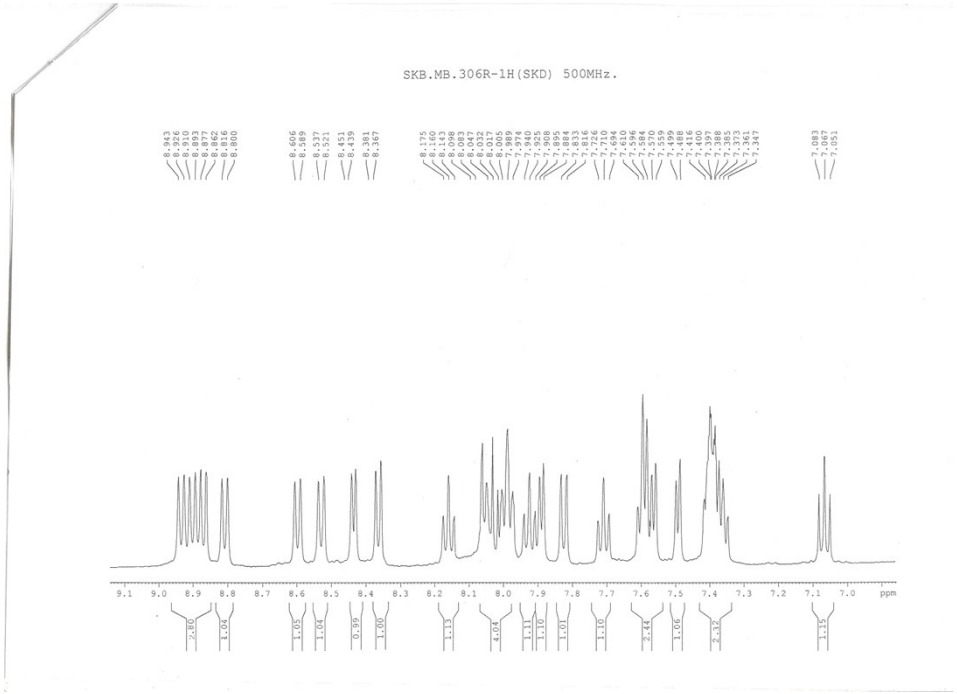

Fig. S7 Scanned ^{1}H NMR spectrum of complex **2** in DMSO-d_6

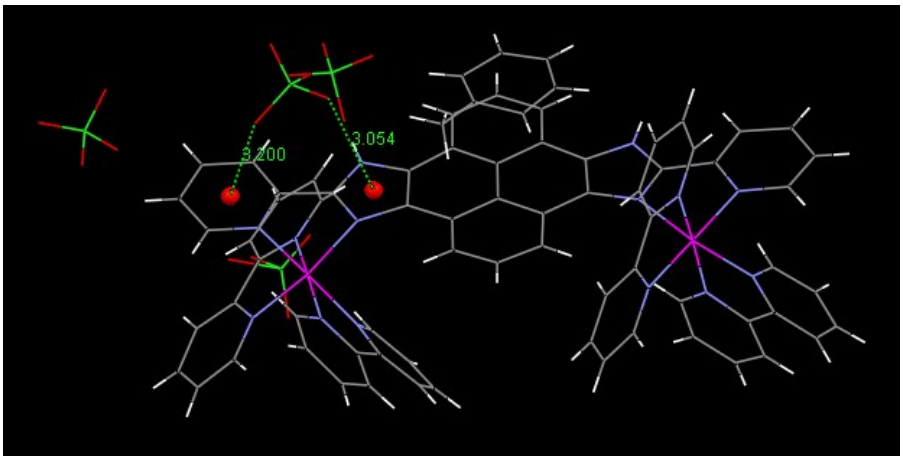

.

Fig. S8 Occurrence of anion-π interaction within **1.**

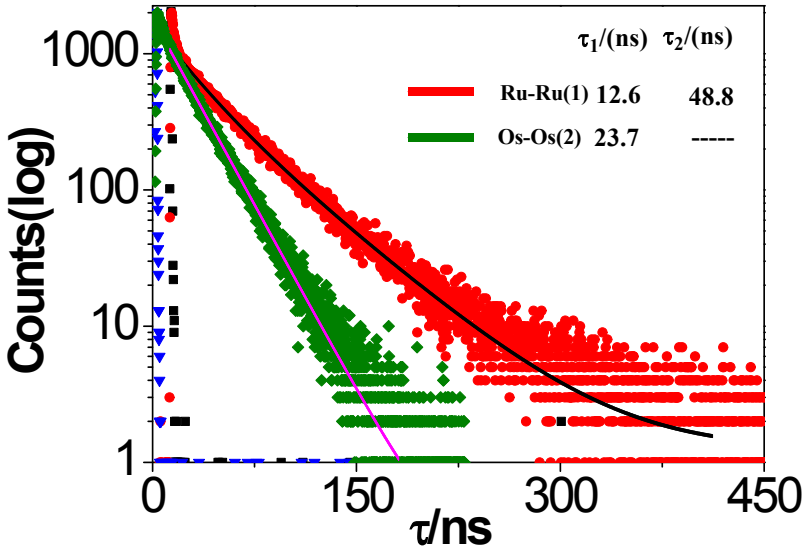

Fig. S9 Time resolved decay profile of **1** and **2** in acetonitrile in their free state. Lifetimes of the complexes were acquired following excitation at 450 nm.

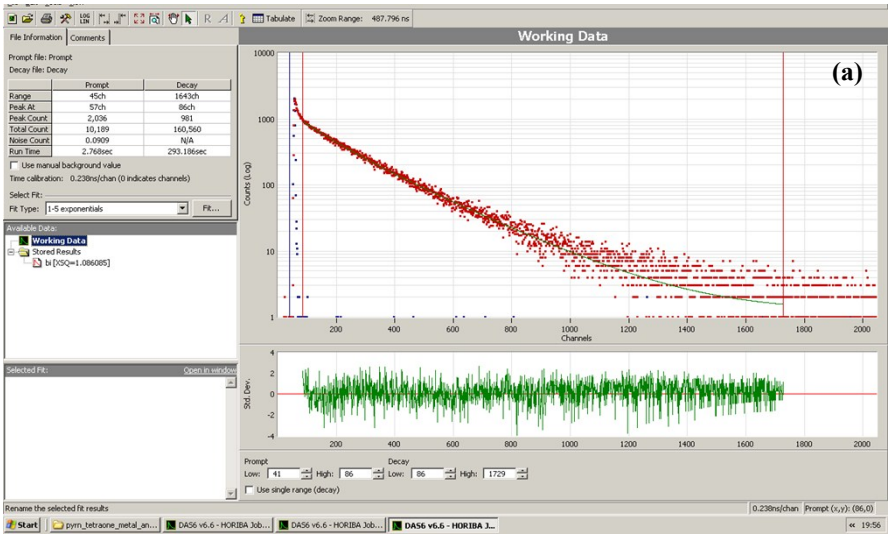


```
---------------------------------
The fitted parameters are:

 Hi reduced to: 1672 ch

 SHIFT = 3.661401E-02 ch
         8.725042E-12 sec
         S.Dev = 1.132722E-10 sec

 T1 = 53.05135 ch
      1.264203E-08 sec
      S.Dev = 1.437123E-09 sec
 T2 = 199.9002 ch
      4.88358E-08 sec
      S.Dev = 2.417946E-10 sec

 A  = 1.617484
      S.Dev = 6.625398E-02

 B1 = 4.368845E-02
      [12.51 Rel.Ampl]
      S.Dev = 1.003443E-03
 B2 = 8.110892E-02
      [87.49 Rel.Ampl]
      S.Dev = 3.004865E-04

 CHISQ = 1.144919
 [ 1595 degrees of freedom ]
```

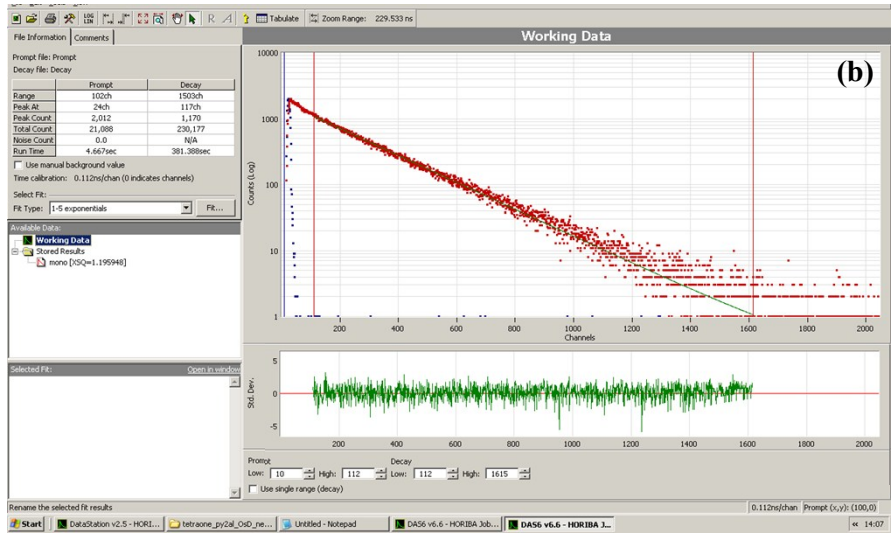


```
---------------------------------
The fitted parameters are:

 SHIFT = 0.4 ch
         4.485248E-11 sec
         S.Dev = 4.485248E-11 sec

 T1 = 212.1192 ch
      2.378518E-08 sec
      S.Dev = 6.840385E-11 sec

 A  = 0.1609985
      S.Dev = 0.0713059

 B1 = 7.701083E-02
      [100.00 Rel.Ampl]
      S.Dev = 1.650364E-04

 CHISQ = 1.195948
 [ 1500 degrees of freedom ]
```

Fig. S10 Fitted images and corresponding statistics of fit for the luminescence decay profile of **1** (a) and **2**(b) respectively in acetonitrile in their free states**.**

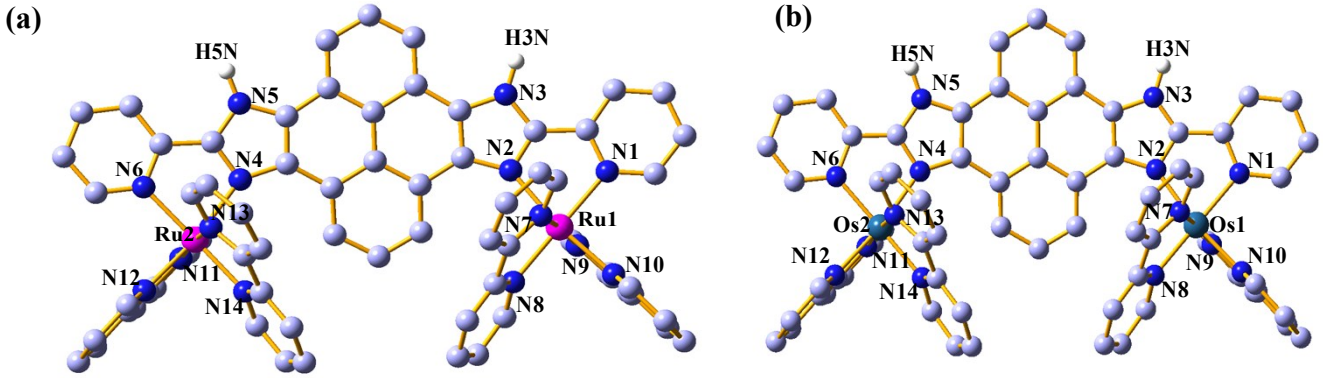

Fig. S11 Optimized geometries and labelling scheme for (a) $[(bpy)_2Ru(H_2Imz_2PPy_2)Ru(bpy)_2]^{4+}$ (**1**) and (b) $[(bpy)_2Os(H_2Imz_2PPy_2)Os(bpy)_2]^{4+}$ (**2**) in solution phase.

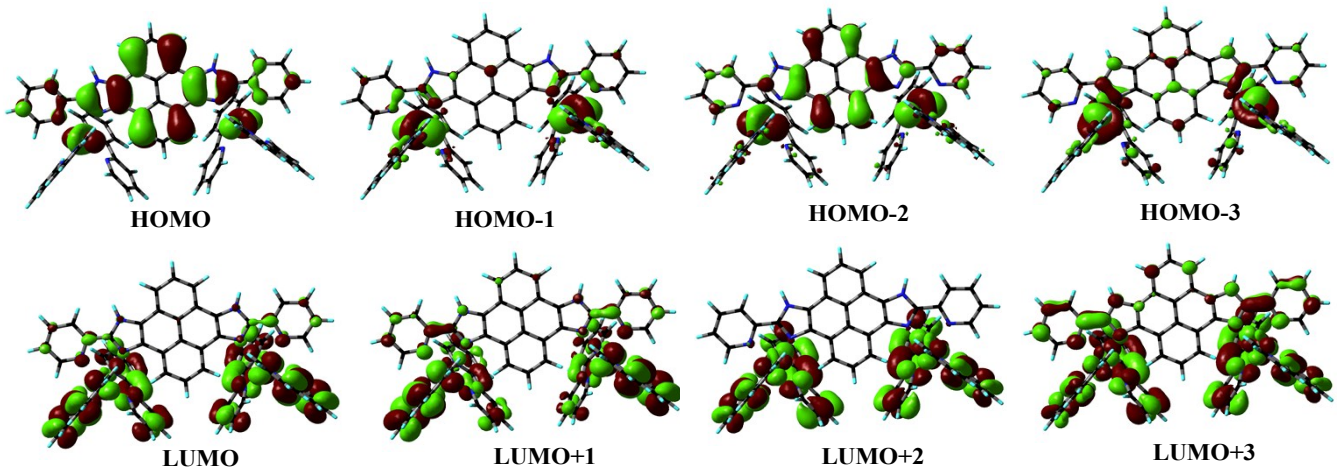

Fig. S12 Schematic drawings of the selective frontier molecular orbitals for $[(bpy)_2Ru(H_2Imz_2PPy_2)Ru(bpy)_2]^{4+}$ (**1**) in solution phase.

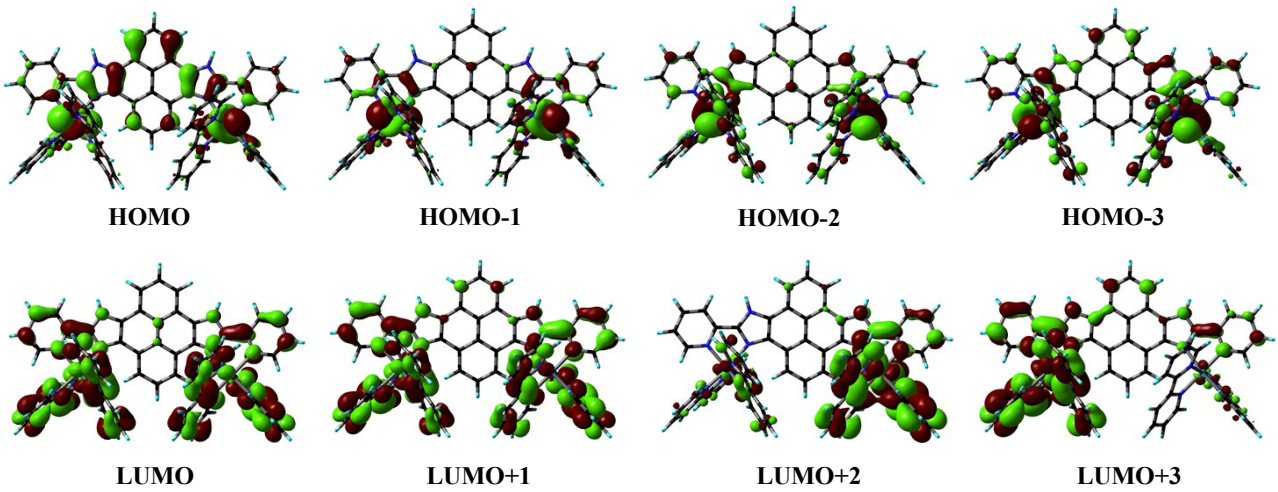

Fig. S13 Schematic drawings of the selective frontier molecular orbitals for $[(bpy)_2Os(H_2Imz_2PPy_2)Os(bpy)_2]^{4+}$ (**2**) in solution phase.

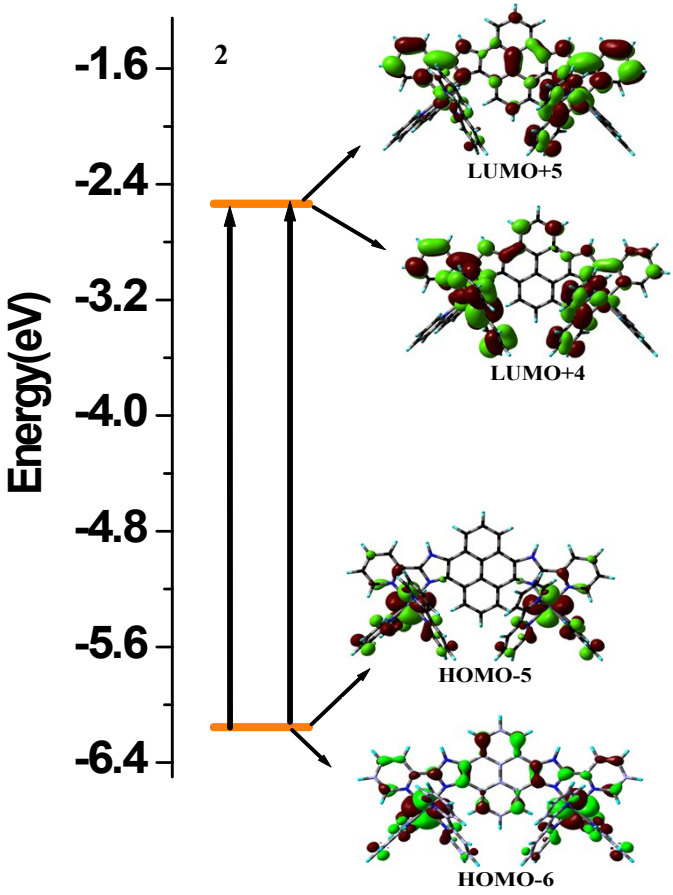

Fig. S14 Energy level diagrams depicting the dominant transitions that comprise the lowest-energy absorption band for $[(bpy)_2Os(H_2Imz_2PPy_2)Os(bpy)_2]^{4+}$ (**2**) in acetonitrile.

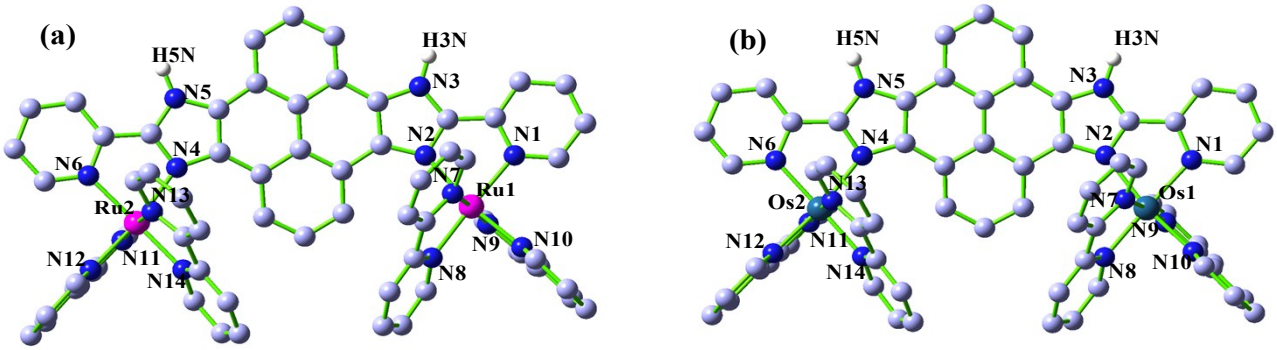

Fig. S15 Optimized geometries and labelling scheme for $[(bpy)_2Ru(H_2Imz_2PPy_2)Ru(bpy)_2]^{4+}$ (**1**) and $[(bpy)_2Os(H_2Imz_2PPy_2)Os(bpy)_2]^{4+}$ (**2**) in UKS state.

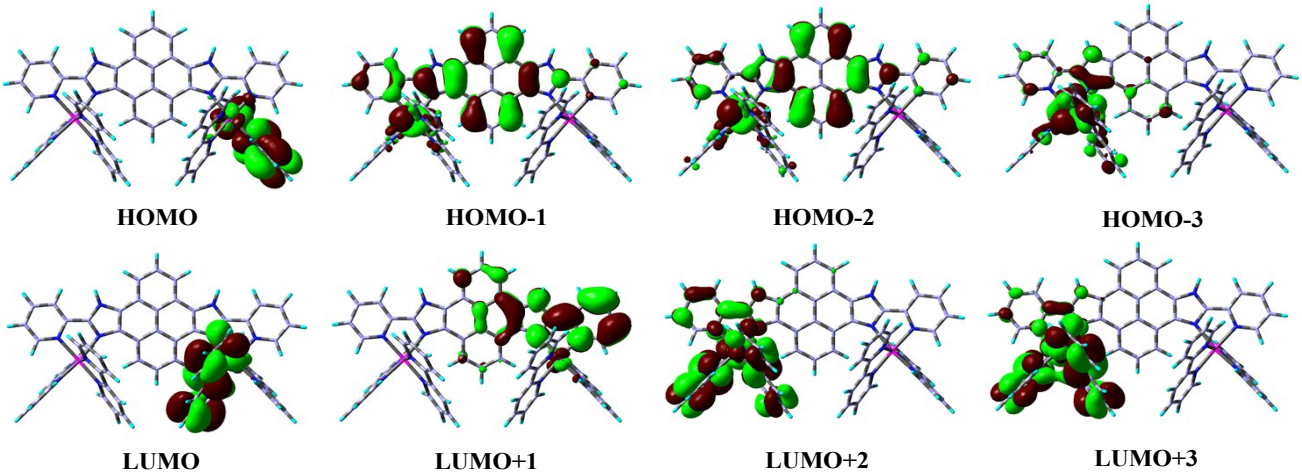

Fig. S16 Schematic drawings of the selective frontier molecular orbitals for $[(bpy)_2Ru(H_2Imz_2PPy_2)Ru(bpy)_2]^{4+}$ (**1**) in UKS optimized state.

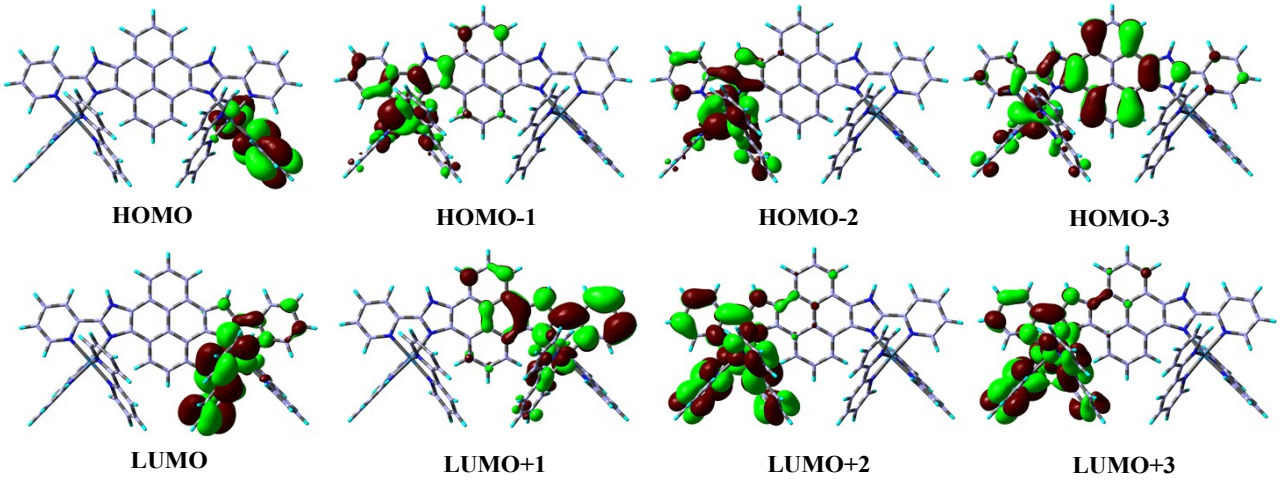

Fig. S17 Schematic drawings of the selective frontier molecular orbitals for $[(bpy)_2Os(H_2Imz_2PPy_2)Os(bpy)_2]^{4+}$ (**2**) in UKS optimized state.

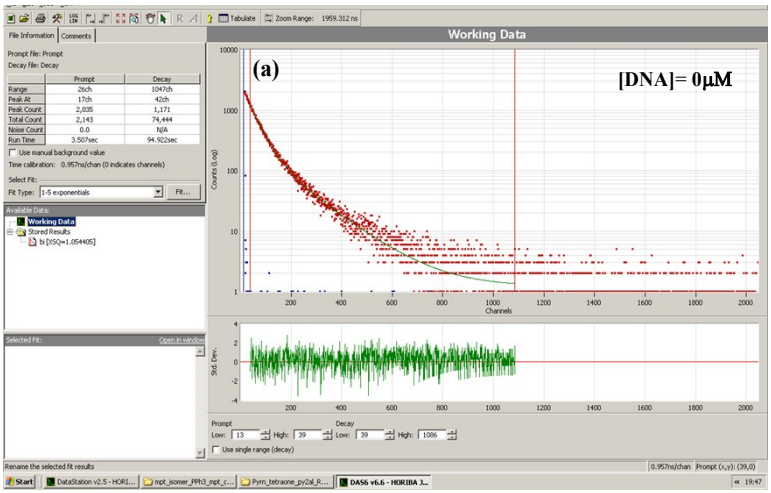


```
---------------------------------
The fitted parameters are:

 SHIFT = 1.9 ch
         1.818609E-09 sec
         S.Dev = 1.69639E-09 sec

 T1 = 42.97166 ch
      4.143087E-08 sec
      S.Dev = 7.184974E-10 sec
 T2 = 144.4753 ch
      1.341863E-07 sec
      S.Dev = 1.83166E-09 sec

 A  = 1.023088
      S.Dev = 5.134795E-02

 B1 = 0.7422737
      [66.34 Rel.Ampl]
      S.Dev = 5.226232E-03
 B2 = 0.1120418
      [33.66 Rel.Ampl]
      S.Dev = 1.130217E-03

 CHISQ = 1.008743
 [ 1253 degrees of freedom ]
```

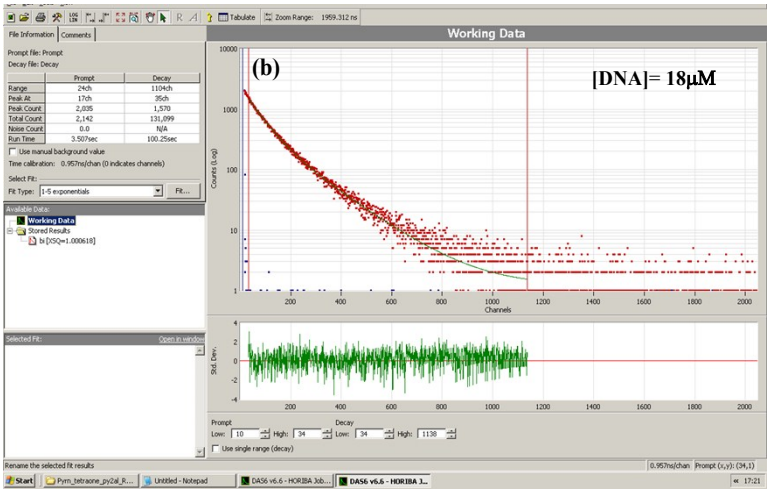


```
The fitted parameters are:

 SHIFT = -8.214164E-02 ch
         -7.862292E-11 sec
         S.Dev = 3.9433E-09 sec

 T1 = 59.02127 ch
      5.429296E-08 sec
      S.Dev = 1.411408E-09 sec
 T2 = 151.5714 ch
      1.650785E-07 sec
      S.Dev = 1.572596E-09 sec

 A  = 1.230422
      S.Dev = 7.701985E-02

 B1 = 0.6455741
      [51.68 Rel.Ampl]
      S.Dev = 5.272183E-03
 B2 = 0.2350785
      [48.32 Rel.Ampl]
      S.Dev = 1.822528E-03

 CHISQ = 1.000618
 [ 1099 degrees of freedom ]
```

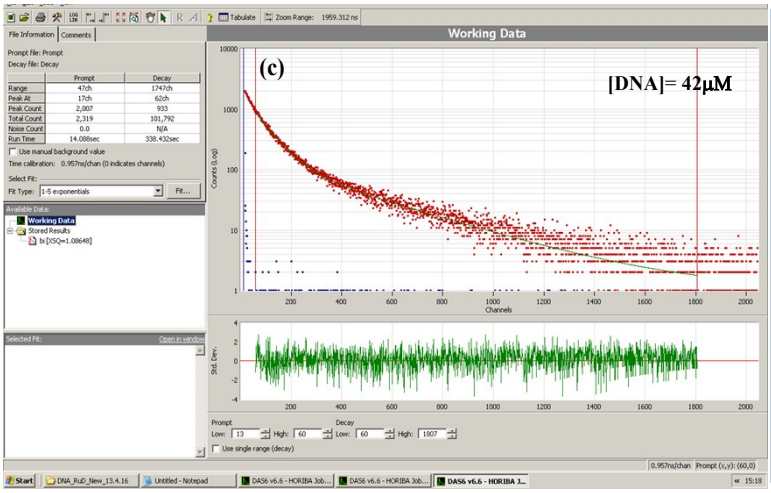


```
The fitted parameters are:

 SHIFT = 2.0327 ch
         1.945625E-09 sec
         S.Dev = 1.285637E-09 sec

 T1 = 67.54663 ch
      6.635312E-08 sec
      S.Dev = 8.873542E-10 sec
 T2 = 335.6617 ch
      3.352829E-07 sec
      S.Dev = 4.446409E-09 sec

 A  = 1.026559
      S.Dev = 6.958518E-02

 B1 = 0.6158694
      [65.10 Rel.Ampl]
      S.Dev = 3.710504E-03
 B2 = 6.645432E-02
      [34.90 Rel.Ampl]
      S.Dev = 5.109302E-04

 CHISQ = 1.08648
 [ 1742 degrees of freedom ]
```

Fig. S18 Fitted images and corresponding statistics for the fit of each of the luminescence decay of **1** (a-c) in presence of increasing amount of CT-DNA in Tris-NaCl buffer medium (pH=7.30).

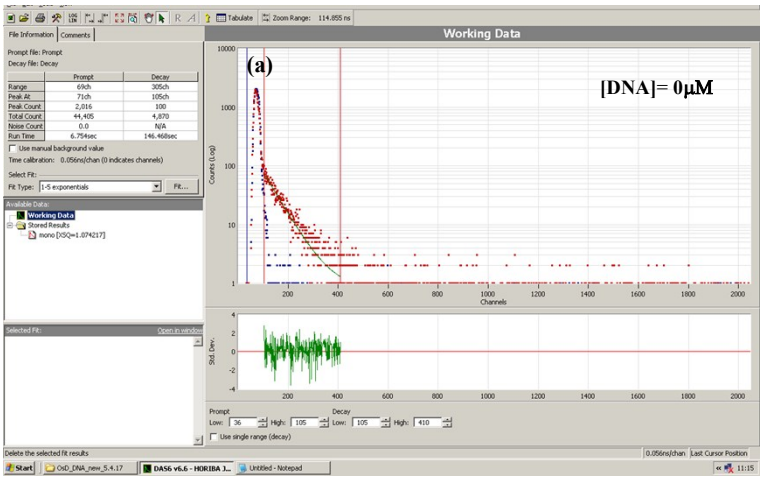

The fitted parameters are:

SHIFT = -6.594157E-02 ch
-3.699905E-12 sec
S.Dev = 1.261805E-10 sec

T1 = 60.13293 ch
3.373989E-09 sec
S.Dev = 1.033712E-10 sec

A = 0.8479583
S.Dev = 0.1325293

B1 = 2.678487E-03
[100.00 Rel.Ampl]
S.Dev = 4.678271E-05

CHISQ = 1.074217
[302 degrees of freedom]

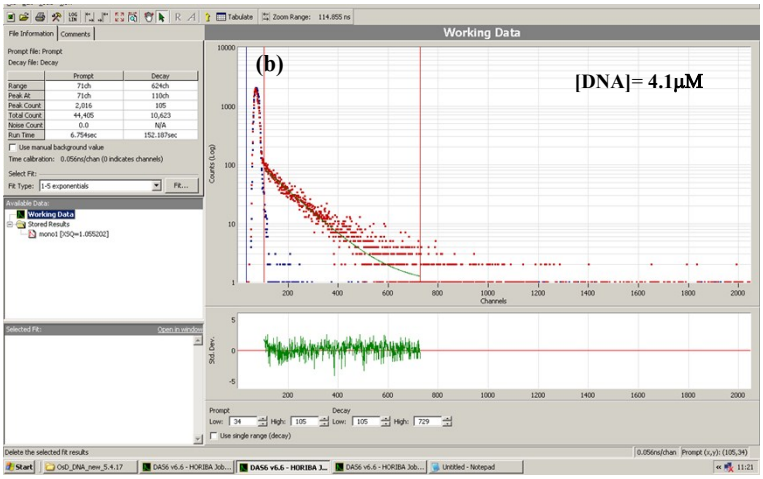

The fitted parameters are:

SHIFT = -0.1310402 ch
-7.352511E-12 sec
S.Dev = 3.349409E-10 sec

T1 = 111.1268 ch
6.235195E-09 sec
S.Dev = 1.135144E-10 sec

A = 0.9556906
S.Dev = 8.709306E-02

B1 = 2.517672E-03
[100.00 Rel.Ampl]
S.Dev = 2.888786E-05

CHISQ = 1.055202
[621 degrees of freedom]

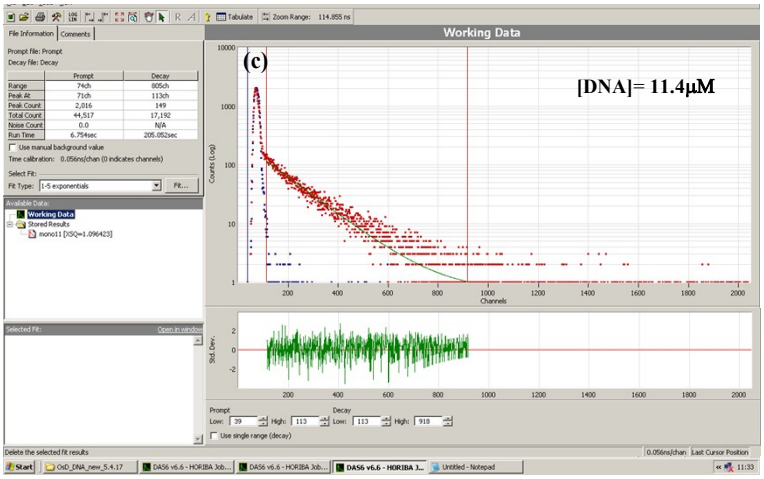

The fitted parameters are:

SHIFT = -5.846859E-02 ch
-3.280605E-12 sec
S.Dev = 2.832513E-10 sec

T1 = 135.5538 ch
7.605765E-09 sec
S.Dev = 1.075715E-10 sec

A = 0.7150995
S.Dev = 7.388485E-02

B1 = 3.48344E-03
[100.00 Rel.Ampl]
S.Dev = 3.001725E-05

CHISQ = 1.096423
[802 degrees of freedom]

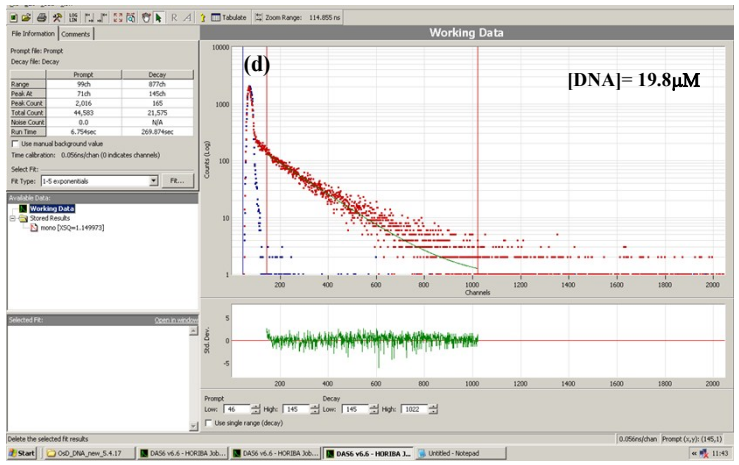


```
The fitted parameters are:

 SHIFT = -9.999993E-02 ch
         -5.61088E-12 sec
         S.Dev = 8.336415E-10 sec

 T1 = 153.2918 ch
      8.601025E-09 sec
      S.Dev = 1.121407E-10 sec

 A  = 0.8411134
      S.Dev = 7.882145E-02

 B1 = 4.62003E-03
      [100.00 Rel.Ampl]
      S.Dev = 3.580114E-05

 CHISQ = 1.149973
 [ 874 degrees of freedom ]
```

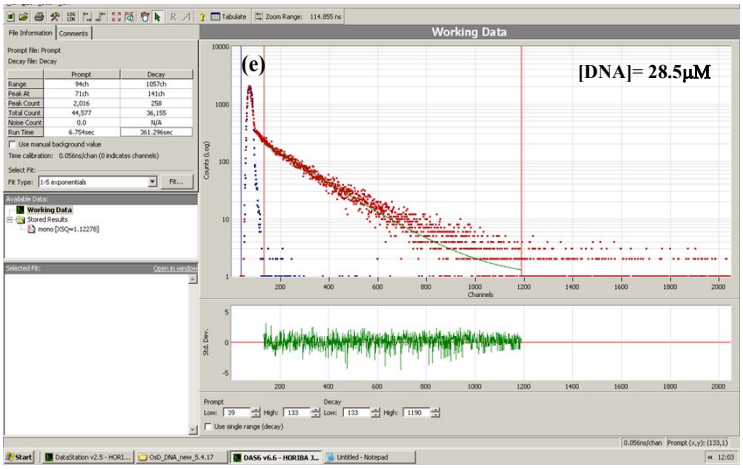


```
The fitted parameters are:

 SHIFT = -9.999999E-02 ch
         -5.610883E-12 sec
         S.Dev = 7.500983E-10 sec

 T1 = 165.403 ch
      9.280567E-09 sec
      S.Dev = 8.477425E-11 sec

 A  = 0.953526
      S.Dev = 7.079282E-02

 B1 = 6.580617E-03
      [100.00 Rel.Ampl]
      S.Dev = 3.789648E-05

 CHISQ = 1.12278
 [ 1054 degrees of freedom ]
```

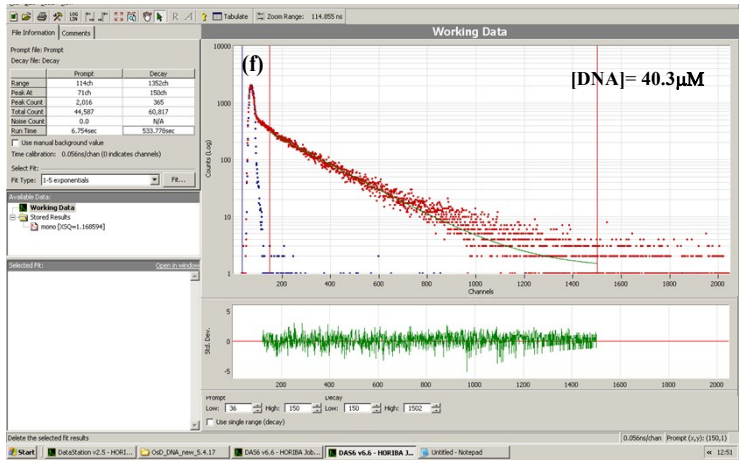


```
The fitted parameters are:

 SHIFT = -0.1 ch
         -5.610884E-12 sec
         S.Dev = 6.517638E-10 sec

 T1 = 190.7604 ch
      1.070335E-08 sec
      S.Dev = 6.548448E-11 sec

 A  = 1.167494
      S.Dev = 5.536998E-02

 B1 = 1.007874E-02
      [100.00 Rel.Ampl]
      S.Dev = 4.354247E-05

 CHISQ = 1.168594
 [ 1453 degrees of freedom ]
```

Fig. S19 Fitted images and corresponding statistics for the fit of each of the luminescence decay of **2** (a-f) in presence of increasing amount of CT-DNA in Tris-NaCl buffer medium (pH=7.30).

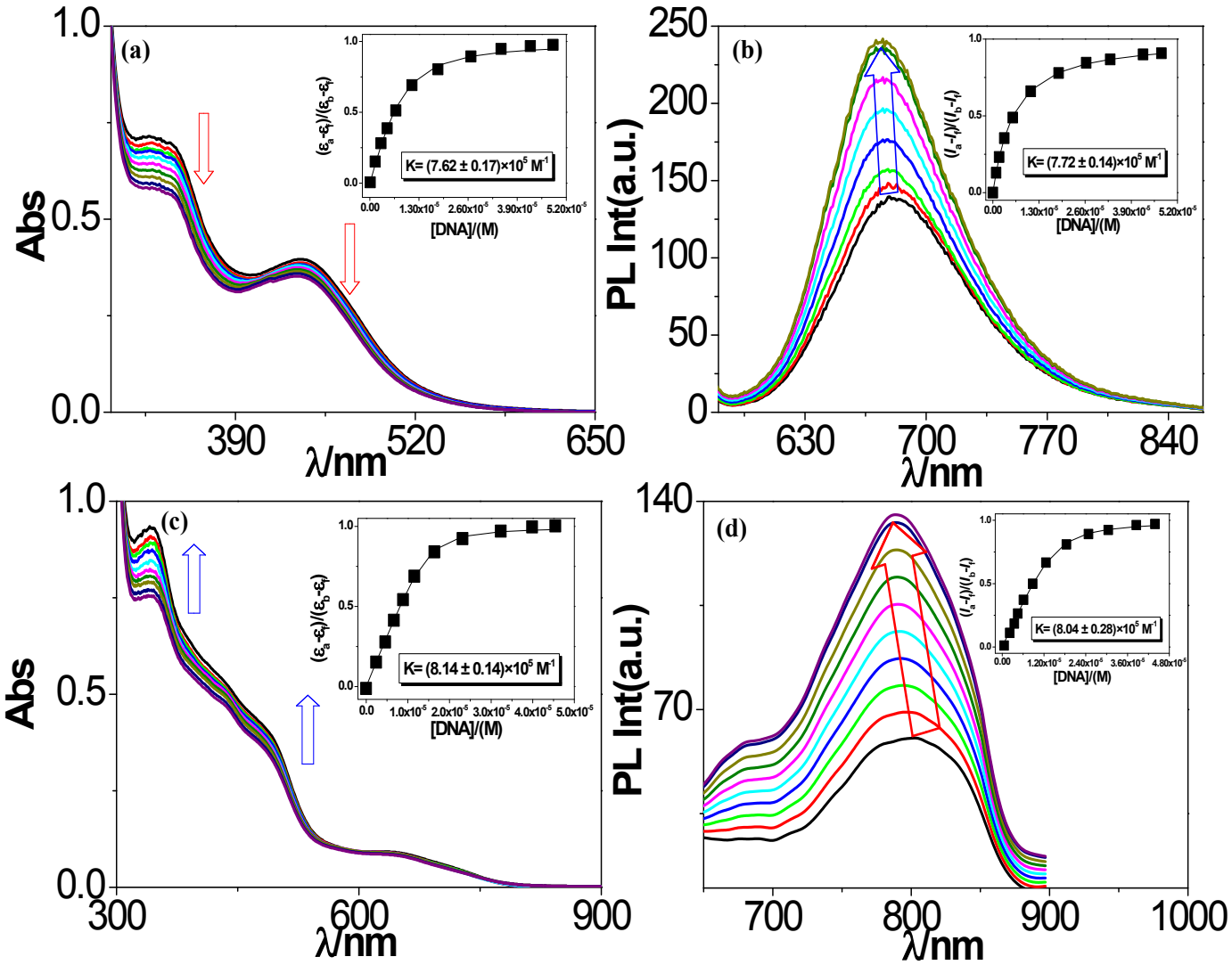

Fig. S20 Changes in UV-vis absorption (a, c) and luminescence spectra (b, d) of **1** and **2** (20μM) in presence of increasing amount of CT-DNA (0-40μM for **1** and 0-36μM for **2**) in 300mM NaCl-Tris buffer medium (pH=7.30). Insets show the binding profile with DNA. Excitation wavelength used for acquiring the luminescence spectra is 450 nm for **1** and 480 nm for **2**.

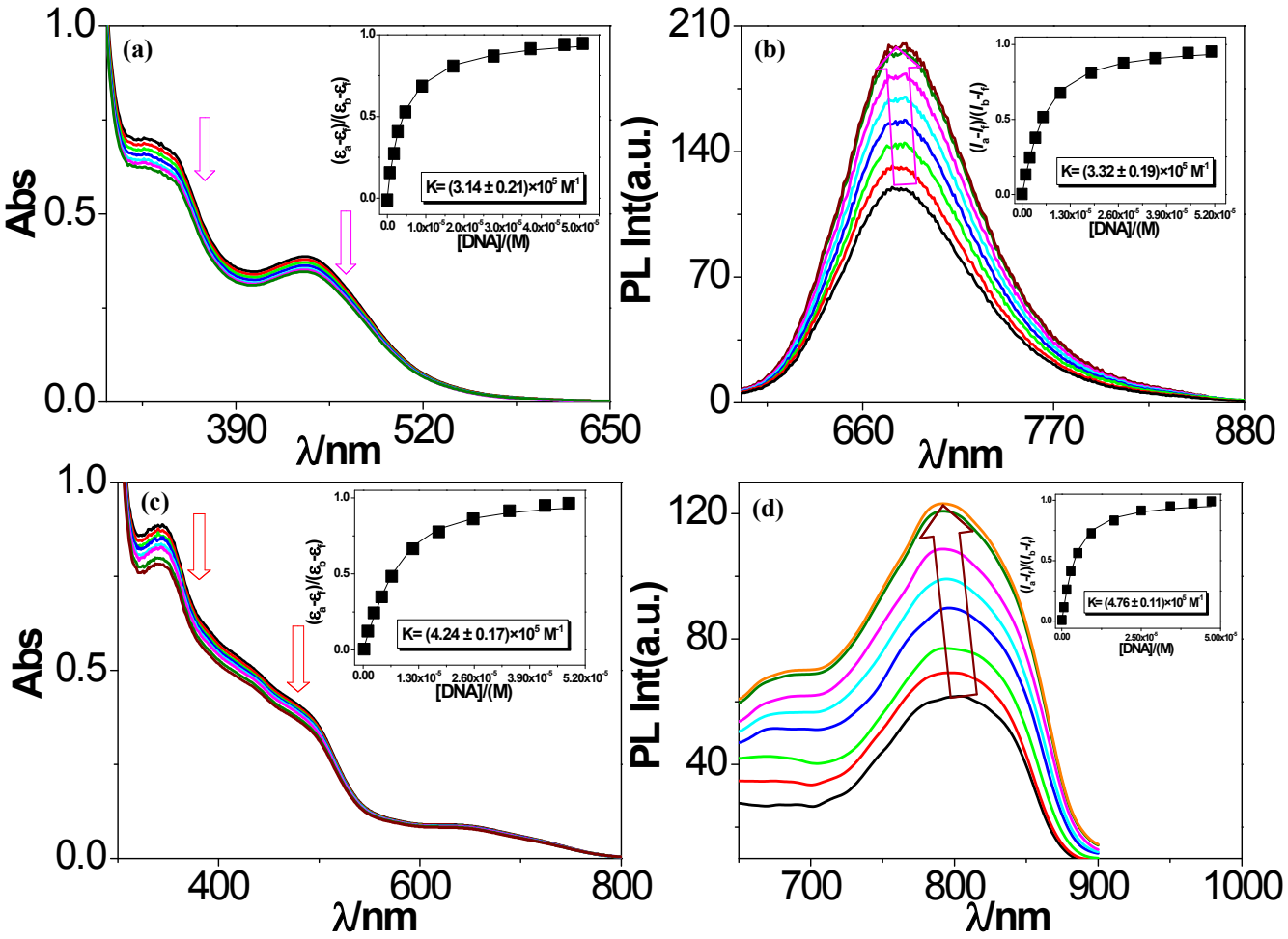

Fig. S21 Changes in UV-vis absorption (a, c) and luminescence spectra (b, d) of **1** and **2** (20μM) in presence of increasing amount of CT-DNA (0-45μM for **1** and 0-40μM for **2**) in 1M NaCl-Tris buffer medium (pH=7.30). Insets show the binding profile with DNA. Excitation wavelength used for acquiring the luminescence spectra is 450 nm for **1** and 480 nm for **2**.

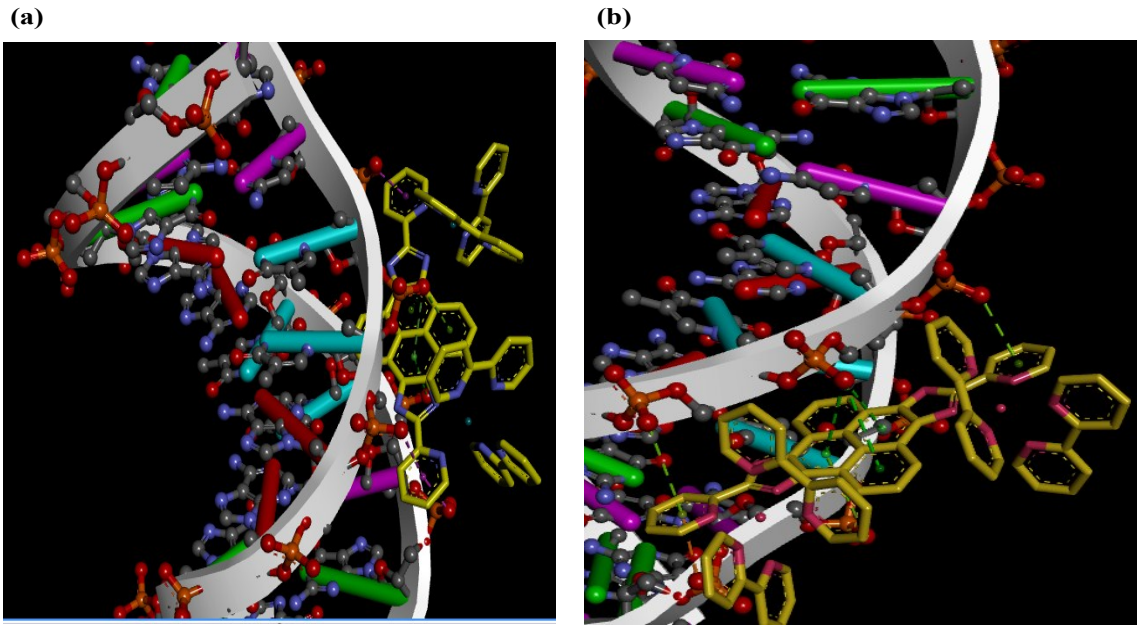

Fig. S22 Occurrence of anion-π interaction between DNA and the complexes; (a) for **1** and (b) for **2**.

References

S1 SAINT (version 6.02), SADABS (version 2.03); Bruker AXS Inc.: Madison, WI, 2002.

S2 SHELXTL, (version 6.10); Bruker AXS Inc.: Madison, WI, 2002.

S3 G. M. Sheldrick, SHELXL-97, *Program for the Refinement of crystal Structures*; University of Göttingen: Göttingen, Germany, 1997.

S4 A. L. Spek, Single-crystal structure validation with the program PLATON. *J. Appl. Cryst.* 2003, **36**, 7-13.

S5 M. J. Frisch, G. W. Trucks, H. B. Schlegel, G. E. Scuseria, M. A. Robb, J. R. Cheeseman, G. Scalmani, V. Barone, B. Mennucci, G. A. Petersson, H. Nakatsuji, M. Caricato, X. Li, H. P. Hratchian, A. F. Izmaylov, J. Bloino, G. Zheng, J. L. Sonnenberg, M. Hada, M. Ehara, K. Toyota, R. Fukuda, J. Hasegawa, M. Ishida, T. Nakajima, Y. Honda, O. Kitao, H. Nakai, T. Vreven, J. A. Jr. Montgomery, J. E. Peralta, F. Ogliaro, M. Bearpark, J. J. Heyd, E. Brothers, K. N. Kudin, V. N. Staroverov, R. Kobayashi, J. Normand, K. A. Rendell, J. C. Burant, S. S. Iyengar, J. Tomasi, M. Cossi, N. Rega, J. M. Millam, M. Klene, J. E. Knox, J. B. Cross, V. Bakken, C. Adamo, J. Jaramillo, R. Gomperts, R. E. Stratmann, O. Yazyev, A. J. Austin, R. Cammi, C. Pomelli, J. W. Ochterski, R. L. Martin, K. Morokuma, V. G. Zakrzewski, G. A. Voth, P. Salvador, J. J. Dannenberg, S. Dapprich, A. D. Daniels, Ö. Farkas, J. B. Foresman, J. V. Ortiz, J. Cioslowski and D. J. Fox, Gaussian 09, revision A.02; Gaussian Inc.: Wallingford, CT, 2009.

S6 A. D. Becke, *J. Chem. Phys.* 1993, **98***,* 5648-5652.

S7 C. T. Lee, W. T. Yang and R. G. Parr, *Phys. Rev. B* 1988, **37**, 785-789.

S8 (a) D. Andrae, U. Haeussermann, M. Dolg, H. Stoll and H. Preuss, *Theor. Chim. Acta.* 1990, **77**, 123-141; (b) P. Fuentealba, H. Preuss, H. Stoll and L. V. Szentpaly, *Chem. Phys. Lett*. 1989, **89**, 418-422.

S9 P. J. Hay and W. R. Wadt, *J. Chem. Phys.* 1985, **82**, 299-310.

S10 M. E. Casida, C. Jamorski, K. C. Casida and D. R. Salahub, *J. Chem. Phys.* 1998, **108**, 4439-4449.

S11 R. E. Stratmann, G. E. Scuseria and M. J. Frisch, *J. Chem. Phys.* 1998, **109**, 8218-8224.

S12 V. A. Walters, C. M. Hadad, Y. Thiel, S. D. Colson, K. B. Wiberg, P. M. Johnson and J. B. Foresman, *J. Am. Chem. Soc.* 1991, **113**, 4782-4791.

S13 (a) J. Tomasi, B. Mennucci and R. Cammi, *Chem. Rev*. 2005, **105**, 2999-3094. (b) M. Cossi, G. Scalmani, N. Rega and V. Barone, *J. Chem. Phys*. 2002, **117**, 43-54.

S14 M. Caricato, B. Mennucci, J. Tomasi, F. Ingrosso, R. Cammi, S. Corni and G. Scalmani, *J. Chem. Phys*. 2006, **124**, 124520-124530.

S15 B. Mennucci, C. Cappelli, C. A. Guido, R. Cammi and J. Tomasi, *J. Phys. Chem. A* 2009, **113**, 3009-3020.

S16 R. II. Dennington, T. Keith and J. Millam, *Gauss View 3*; Semichem, Inc.: Shawnee Mission, KS, 2007.

S17 N. M. O Boyle, A. L. Tenderholt, K. M. Langner, *J. Comput. Chem*. **2008**, *29*, 839-845.

S18 (a) J. D. McGhee and P. H. von Hippel, *J. Mol. Biol*., 1974, **86**, 469-489; (b) R. B. Nair, E. S. Teng, S. L. Kirkand and C. J. Murphy, *Inorg. Chem.,* 1998, **37**, 139-141; (c) R. B. Naira and C. J. Murphy, *J. Inorg. Biochem.* 1998, **69**, 129-133.

S19 M. T. Cater, M. Rodrigueza and A. J. Bard, *J. Am. Chem. Soc*. 1989, **111**, 8901-8911.

S20 D. L. Boger, B. E. Fink, S. R. Brunette, W. C. Tse and M. P. Hedrick, *J. Am. Chem. Soc.* 2001, **123**, 5878-5891.

S21 S. Das, S. Parveena and A. B. Pradhan, *Spectrochimica Acta Part A*: *Molecular and Biomolecular Spectroscopy.* 2014**, 118**, 356-366.

S22 D. Mustard and D. W. Ritchie, *Proteins: Struct. Funct. Bioinf.* 2005, **60**, 269-274.

S23 D. V. Partyka, R. J. Staples and R. H. Holm, *Inorg. Chem*., 2003, **42**, 7877–7886.